THE JOURNAL OF PHYSICAL CHEMISTRY Letters

pubs.acs.org/JPCL Letter

Competing Interactions of Fatty Acids and Monoglycerides Trigger Synergistic Phospholipid Membrane Remodeling

Bo Kyeong Yoon, Soohyun Park, Gamaliel J. Ma, Kavoos Kolahdouzan, Vladimir P. Zhdanov, Joshua A. Jackman,* and Nam-Joon Cho*

Cite This: J. Phys. Chem. Lett. 2020, 11, 4951−4957 Read Online

ACCESS | Metrics & More | Article Recommendations | Supporting Information

Downloaded via NANYANG TECHNOLOGICAL UNIV on June 19, 2020 at 03:34:40 (UTC).
See https://pubs.acs.org/sharingguidelines for options on how to legitimately share published articles.

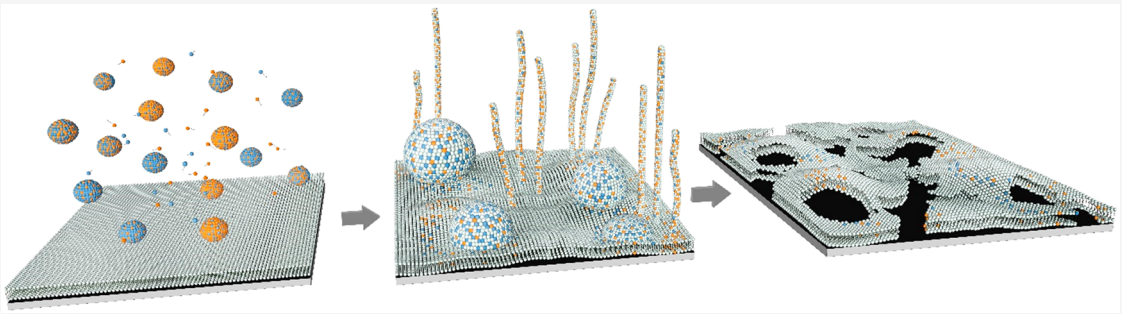

ABSTRACT: Using quartz crystal microbalance-dissipation and time-lapse fluorescence microscopy, we demonstrate that adding mixtures of lauric acid (LA) and glycerol monolaurate (GML), two of the most biologically active antimicrobial fatty acids and monoglycerides, to a supported lipid bilayer triggers concurrent tubule and bud formation, which unexpectedly results in synergistic phospholipid membrane remodeling that far exceeds the effects of GML or LA alone. Together, GML and LA drive pearling instability, dynamic transformation of buds into tubules and vice versa, and extensive membrane lysis. The most pronounced effects occurred with equimolar concentrations of GML and LA, highlighting that synergistic membrane disruption arises from competition for the lipid supply to buds and tubules and an inability to relieve membrane strains. These findings offer a conceptually new model to explain how fatty acid and monoglyceride interactions can trigger phospholipid membrane remodeling events relevant to various biophysical and biological systems.

Understanding how single-chain lipid amphiphiles such as fatty acids and monoglycerides interact with phospholipid membranes is broadly relevant to numerous scientific topics such as pathogen inhibition,[1] biofuel production,[2] and molecular evolution.[3] Medium-chain saturated fatty acids and monoglycerides, especially the 12-carbon long lauric acid (LA) and its monoglyceride derivative glycerol monolaurate (GML), exhibit particularly high levels of membrane-disruptive antimicrobial effects[4] and immune cell interactions.[5] Fatty acids and monoglycerides have also been observed to induce morphological changes in supported lipid bilayers (SLBs).[6,7] In particular, GML and LA are responsible for membrane budding and tubule formation, respectively, in both single-component phospholipid and more complex phospholipid−cholesterol SLBs.[8,9] However, it is far less understood at a physicochemical level how mixtures of fatty acids and monoglycerides interact with and disrupt phospholipid membranes despite reports of synergistic biological activities, such as more potent antibacterial activity of GML/LA mixed micelles compared to GML or LA micelles.[10] To unravel the corresponding processes, we have studied the micellar aggregation properties of different GML/LA mixtures by fluorescence spectroscopy and then explored the interaction of GML/LA micelles with SLBs by quartz crystal microbalance-dissipation (QCM-D) and time-lapse fluorescence microscopy imaging experiments (Scheme 1).

GML/LA mixtures were prepared by varying the molar ratio of the two components in solution (100/0, 80/20, 60/40, 40/60, 20/80, and 0/100 mol % GML/LA), and the critical micelle-formation concentration (CMC) of each GML/LA mixture was first determined. Fluorescence spectroscopy experiments were conducted using the 1-pyrenecarboxaldehyde probe to detect the onset of micelle formation. There was a decrease in the maximum-intensity emission wavelength of the fluorescent probe upon partitioning into the hydrophobic interior of micelles, which has a lower dielectric constant than the aqueous medium.[11] The results demonstrated a strong

Received: April 13, 2020
Accepted: June 1, 2020
Published: June 1, 2020

ACS Publications © XXXX American Chemical Society

https://dx.doi.org/10.1021/acs.jpclett.0c01138
J. Phys. Chem. Lett. 2020, 11, 4951−4957

Scheme 1. Experimental Strategy to Characterize the Membrane-Interaction Profiles of GML/LA Mixtures

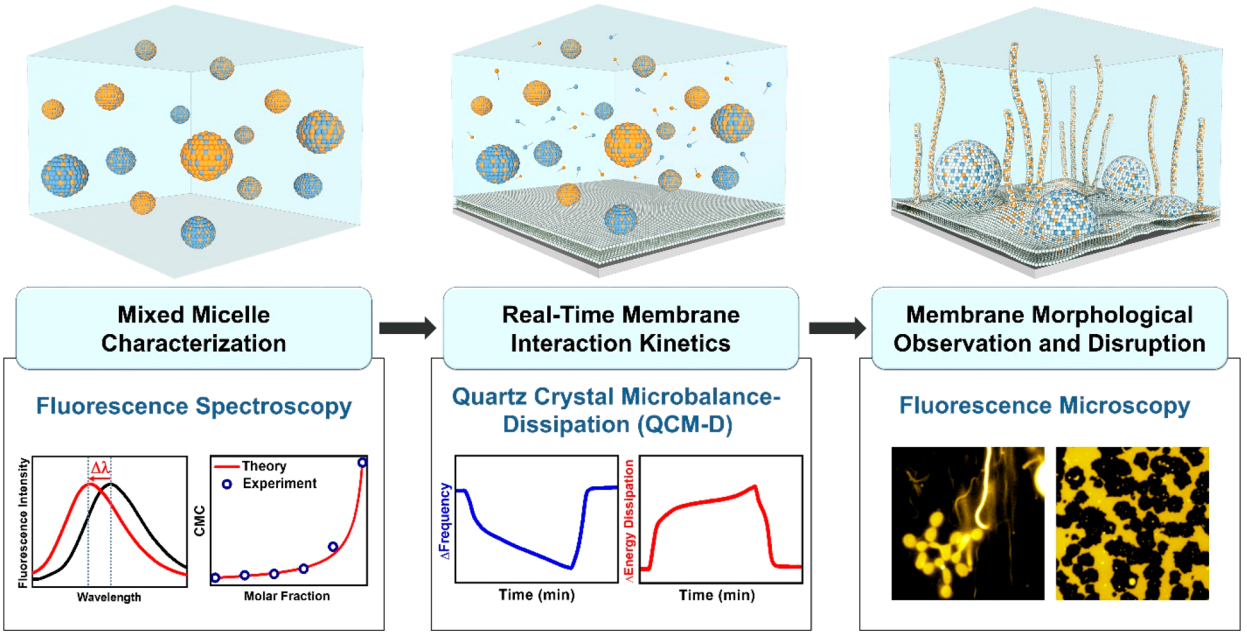

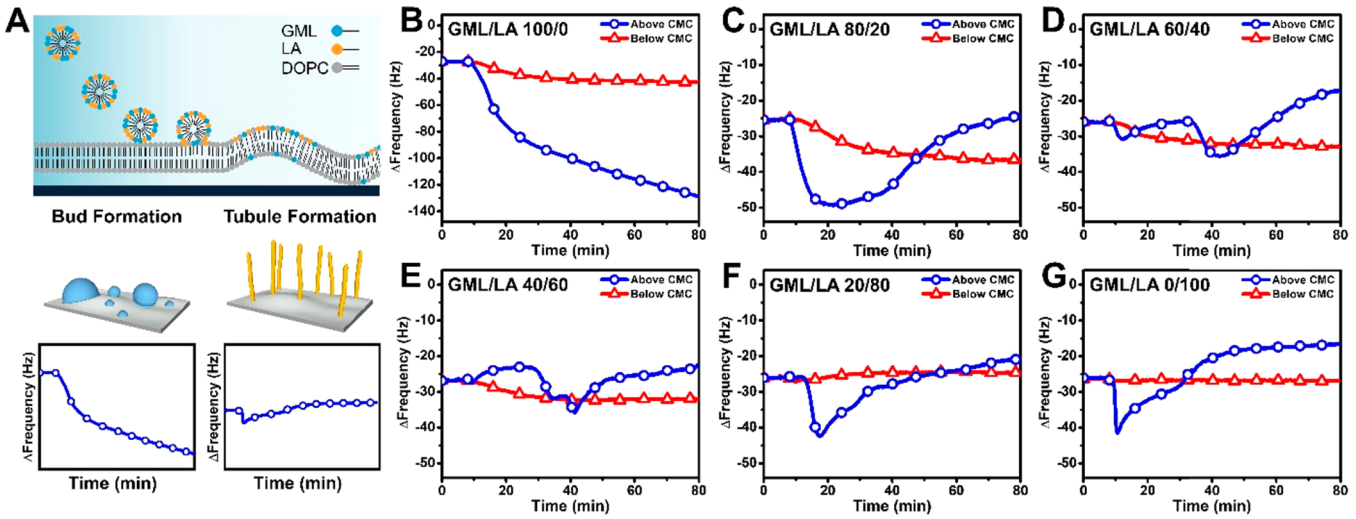

Figure 1. Real-time QCM-D characterization of GML/LA mixture interaction with SLB platforms. (A) Schematic illustration of QCM-D frequency shifts associated with membrane budding and tubule formation. (B–G) Time-resolved frequency shifts for the addition of GML/LA micelles (2 × CMC, blue circles) or GML/LA monomers (0.5 × CMC, red triangles) to DOPC SLB platforms at different molar ratios: (B) 100/0; (C) 80/20; (D) 60/40; (E) 40/60; (F) 20/80; and (G) 0/100 GML/LA. The initial measurement values at t = 0 min correspond to a DOPC SLB platform on a silica-coated sensor surface. GML/LA mixtures were added at t = 10 min after an initial baseline period in equivalent buffer solution.

dependence of CMC on the GML/LA molar ratio. The CMCs of 100/0, 80/20, and 60/40 mol % GML/LA samples were 60, 80, and 90 μM, respectively, while larger CMCs occurred at higher LA fractions (Figure S1). The CMCs of 40/60, 20/80, and 0/100 mol % GML/LA samples were 130, 300, and 950 μM, respectively. The observed trend in CMCs was analyzed using a pseudophase separation model[12] and indicated that GML and LA exhibit ideal mixing and form mixed micelles with well-controlled molar ratios (Figure S2 and section 2 in the Supporting Information).

We then investigated the interaction of GML/LA mixtures with zwitterionic 1,2-dioleoyl-*sn*-glycero-3-phosphocholine (DOPC) SLBs by using the QCM-D technique. For reference, we categorized the QCM-D frequency response profiles associated with individually adding GML or LA to a DOPC SLB, which causes membrane budding or tubule formation, respectively[8] (Figure 1A). The QCM-D frequency signal is sensitive to the hydrodynamically coupled adsorbed mass of the lipid adlayer near the sensor surface (within ~250 nm),[13] and the specific response profile depends on the shape of buds and tubules that evolve from the SLB and corresponding surface sensitivity of the QCM-D frequency signal to the bud and tubule morphologies.[14]

In general, the GML/LA mixtures were significantly more active above the corresponding CMC. For 100 mol % and 80/20 mol % GML/LA micelles, membrane budding was detected (Figure 1B,C). In marked contrast, 60/40 and 40/60 mol % GML/LA micelles induced more complex membrane-interaction profiles, as indicated by a rapid series of modest frequency increases and decreases in successive fashion (Figure

https://dx.doi.org/10.1021/acs.jpclett.0c01138
J. Phys. Chem. Lett. 2020, 11, 4951−4957

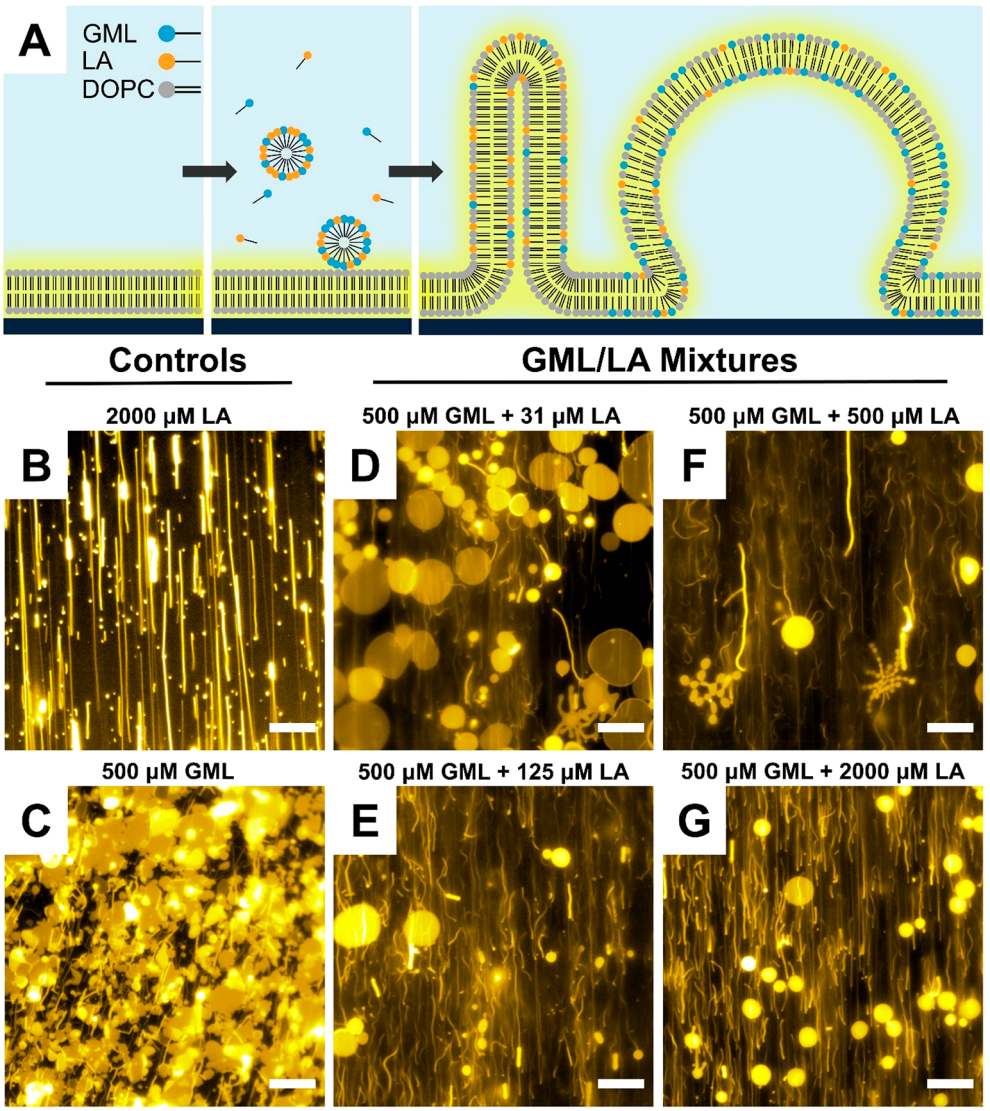

Figure 2. Fluorescence microscopy imaging of membrane morphological changes in SLBs triggered by GML/LA addition (the angle of view with respect to the support is 90°; note that tubules are tilted in the flow direction). (A) Schematic illustration of experimental stages. Representative image snapshots of SLB platforms were recorded around t = 10 min post-GML/LA addition for (B and C) control experiments with 2000 μM LA or 500 μM GML alone, and different GML/LA mixtures as follows: (D) 500 μM GML and 31 μM LA; (E) 500 μM GML and 125 μM LA; (F) 500 μM GML and 500 μM LA; and (G) 500 μM GML and 2000 μM LA. Scale bars: 20 μm.

1D,E). On the other hand, 20/80 and 0/100 mol % GML/LA micelles induced tubule formation (Figures 1F,G). Thus, GML/LA micelles with high GML or LA fractions behaved more similarly to GML or LA micelles, respectively, while GML/LA micelles with similar GML and LA fractions exhibited more complex membrane-interaction profiles (see also Figure S3).

Time-lapse fluorescence microscopy imaging experiments were also conducted in order to directly observe SLB membrane morphological changes (Figure 2A). After SLB formation, we added GML/LA mixtures with fixed 500 μM GML concentration and variable amounts of LA (between 31 μM and 2000 μM) or 500 μM GML or 2 mM LA alone as controls and observed membrane remodeling events.

As expected, the addition of 2000 μM LA or 500 μM GML alone principally induced the formation of elongated tubules or spherical membrane buds (emanating from entangled tubules[8]), respectively (Figure 2B,C and Movies S1 and S2). However, the membrane remodeling events became more complex when GML and LA were added together. The coaddition of 500 μM GML and 31 μM LA mainly triggered membrane budding, but some of the buds had protruding, web-like invaginations (Figure 2D and Movie S3). Moreover, the coaddition of 500 μM GML and 125 μM LA led to the coexistence of elongated tubules and spherical buds with continually evolving shape structures (Figure 2E and Movie S4).

The most distinct membrane morphological changes were observed when 500 μM GML and 500 μM LA were added together. The initial coexistence of elongated tubules and spherical buds preceded more dynamic changes whereby several buds began to exhibit pearling behavior[15] (Figure 2F and Movie S5). On the other hand, the coaddition of 500 μM GML and 2000 μM LA mainly triggered the formation of elongated tubules and some buds, which appeared to stably coexist unlike at the more intermediate GML/LA ratios (Figure 2G and Movie S6). Thus, the data support that GML/LA mixtures can trigger a wide range of membrane

https://dx.doi.org/10.1021/acs.jpclett.0c01138
J. Phys. Chem. Lett. 2020, 11, 4951−4957

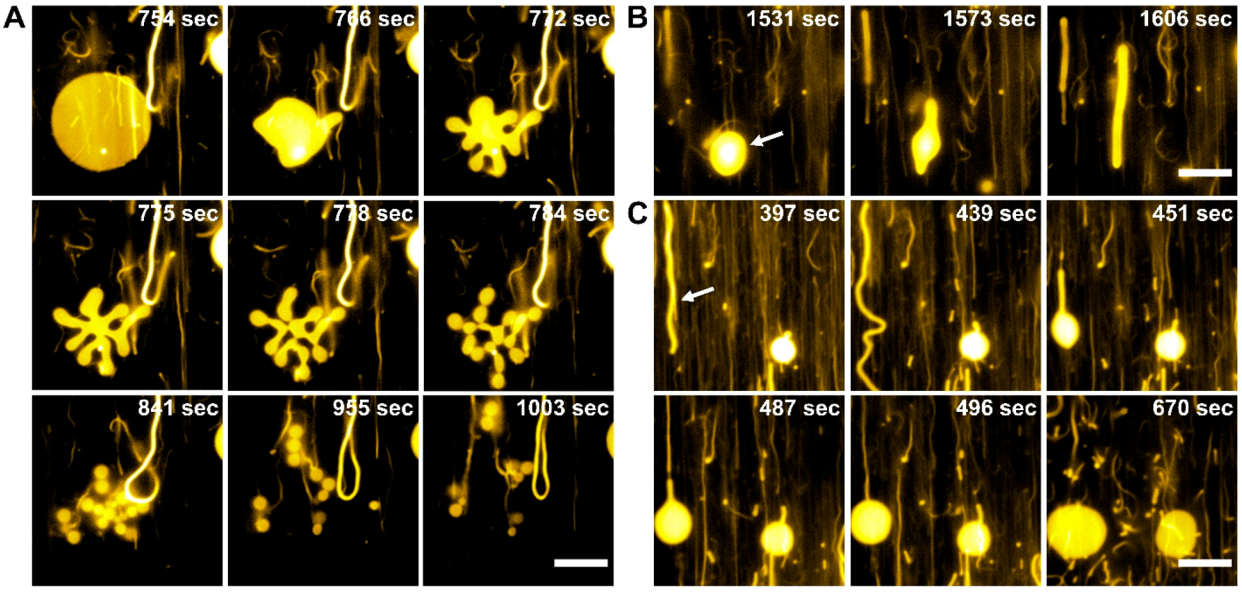

Figure 3. Dynamic shape transformations of supported lipid membranes and pearling instability. GML/LA mixtures were added to a fluorescently labeled DOPC SLB. (A) A spherical bud protrusion formed upon addition of a 500/500 μM GML/LA mixture. Eventually, the bud transformed shape and the dynamic process lasted around 5 min. (B) A spherical bud protrusion initially formed upon addition of a 500/500 μM GML/LA mixture. Eventually, the bud rapidly transformed into a tubule. (C) A tubular protrusion initially formed upon addition of a 500/125 μM GML/LA mixture. Eventually, the tubule rapidly transformed into a bud. For panels A–C, image snapshots are presented at different time points during the respective shape transformations. The time stamp on each image indicates the time elapsed after GML/LA addition. In applicable cases, white arrows indicate lipid structures of interest. Scale bars: 15 μm.

morphological changes that exceeds what occurs with GML or LA alone.

The pearling behavior exhibited in the equimolar mixture of 500 μM GML and 500 μM LA case is a key example of how GML/LA mixtures induce dynamic membrane morphological changes. The corresponding time-lapse snapshots depict how an initially formed bud transforms shape into pearls-on-a-string and subsequently breaks down (Figure 3A and Movie S7). After ~12 min, a large spherical bud of ~30 μm diameter began to exhibit instability, as indicated by loss of spherical structure and formation of web-like protrusions. The protrusions evolved into pearls-on-a-string, and structural integrity was compromised within ~2 min thereafter.

We also observed the rapid conversion of spherical buds into elongated tubules and vice versa in the case of GML/LA mixtures at intermediate molar ratios. In Figure 3B, a spherical bud of ~10 μm diameter formed upon the coaddition of 500 μM GML and 500 μM LA is depicted to convert rapidly into a tubule within a short time period of ~1 min (Movie S8). In another example, an elongated tubule formed upon the coaddition of 500 μM GML and 125 μM LA is shown to evolve into a spherical bud (Figure 3C and Movie S9). By contrast, neither pearling instability nor interconversion of buds and tubules was observed in predominately GML or LA samples.

To further characterize the interaction of GML/LA mixtures with SLB platforms, we investigated the effect of GML/LA treatment on the membrane integrity of fluorescently labeled DOPC SLBs. The addition of 2000 μM LA or 500 μM GML caused a low degree of membrane defects (Figures 4A,B and Movies S10 and S11). By contrast, the addition of GML/LA mixtures, consisting of 500 μM GML plus varying amounts of LA, caused more extensive membrane lysis. Specifically, the coaddition of 500 μM GML plus 31 or 125 μM LA caused appreciably more membrane damage than GML or LA alone (Figures 4C,D and Movies S12 and S13). The most extensive damage occurred when 500 μM GML and 500 μM LA were added together, while more moderate damage occurred when 500 μM GML and 2000 μM LA were added together (Figure 4E,F and Movies S14 and S15). The surface area percentage of membrane defects within the SLBs verified that the coaddition of 500 μM GML and 500 μM LA caused the most extensive damage, amounting to around 58 ± 1.0% of the total surface area (Figure 4G). By contrast, the coaddition of 500 μM GML and 2000 μM LA damaged around 25 ± 3.2% of the total surface area, which was much lower than even when 500 μM GML and 125 μM LA were added together (43 ± 1.4%). The data support that (i) adding higher total amounts of GML and LA does not always increase the extent of membrane lysis and (ii) the highest levels of membrane lysis occurred at intermediate GML/LA molar ratios.

Concerning the underlying physics, we note that in two- or multicomponent suspended membranes, the suitable generic mechanism of bud formation is related to phase separation, i.e., the appearance of domains, provided they have appreciable spontaneous curvature whereby the observed curvature is determined by a trade-off between the bending and boundary energies (see the seminal studies[16,17] by Jülicher and Lipowsky, recent review,[18] and references in section 3 of the Supporting Information). With suitable modification, this mechanism is also operative for describing tubule formation along with both scenarios in the presence of a solid support as well. Our fluorescence microscopy data indicate that the buds contain primarily GML and DOPC, while the tubules are composed primarily of LA and DOPC. The flat SLB contacting the support contains DOPC and may contain GML and LA. The energy of the corresponding membrane patches includes (i) lateral interactions between DOPC, GML, and LA molecules

https://dx.doi.org/10.1021/acs.jpclett.0c01138
J. Phys. Chem. Lett. 2020, 11, 4951–4957

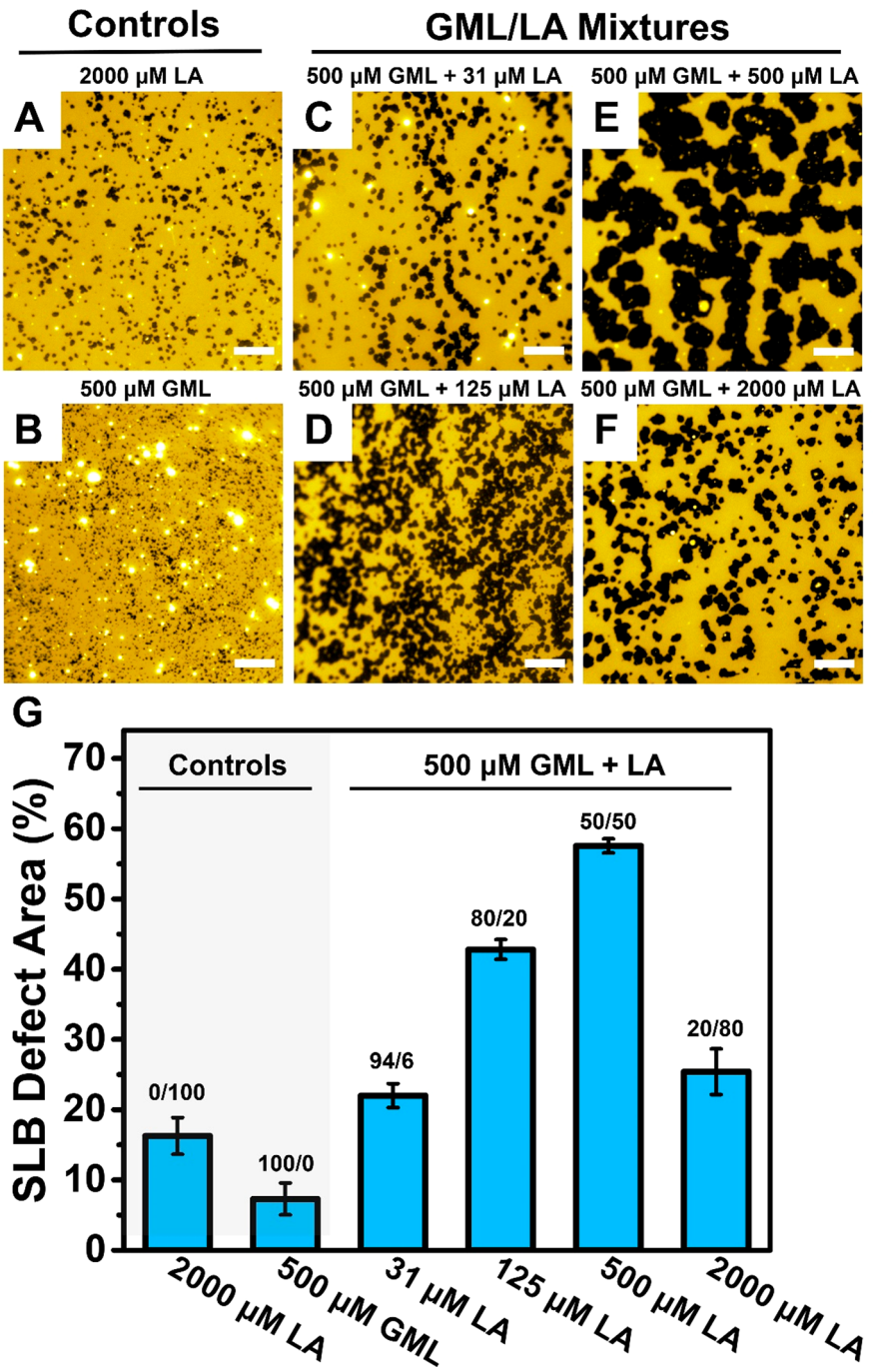

Figure 4. Quantitative comparison of membrane lysis caused by GML/LA mixtures. (A and B) Control experiments with 2000 μM LA or 500 μM GML. (C−F) GML/LA mixture experiments for different GML/LA molar ratios. (G) Surface area percentage of membrane defects in SLBs for data in panels A−F. The GML/LA molar ratio is indicated on top of each column. Mean ± standard deviation is reported for n = 5 replicates per test group. Scale bars: 20 μm.

within the bilayer, (ii) bilayer bending energy, and (iii) bilayer−substrate interactions, respectively (see also section 3 in the Supporting Information). The formation of different phases is related primarily to appreciable attractive lateral DOPC-GML and DOPC-LA interactions. The shape of the patches not contacting the support depends on the spontaneous curvature. If the lateral interaction is isotropic, then the spontaneous curvature is isotropic as well, and if this curvature is appreciable, then the corresponding model will describe bud formation as we observe in the GML case. If the lateral interaction is strongly anisotropic, then the spontaneous curvature will also be anisotropic; i.e., the formation of the membrane curvature with respect to one of the axes will make curvature formation less favorable with respect to the other axis. If this effect is appreciable, i.e., the curvature is appreciable only with respect to one of the directions, then the model will predict tubule formation as we observe in the LA case. Physically, the spontaneous curvature is related to the length difference between DOPC, GML, and LA molecules and the specifics of their hydrophilic heads (Figure S4), as well as the different compositions of the external and internal leaflets of a membrane.

https://dx.doi.org/10.1021/acs.jpclett.0c01138
J. Phys. Chem. Lett. 2020, 11, 4951−4957

The bud- and tubule-forming phases are more stable compared to the patches contacting the support, because we observe their growth as long as there is supply of GML and LA from the solution and supply of DOPC from the patches contacting the support. In the QCM-D measurements, the bud formation is clearly manifested in the initial decrease of the QCM-D frequency shift (i.e., in the increase of its absolute value). For coadsorbed GML and LA, the GML-containing buds and LA-containing tubules first grow almost independently because DOPC is in excess, and at the equimolar GML/LA ratio, both these processes are well manifested. Then, the growth of buds is followed by their partial decomposition related to the consumption of DOPC by growing tubules. This means that the strength of the DOPC-LA lateral interaction in tubules is larger than that of the DOPC-GML interaction in buds, but not dramatically larger, because some of the buds are still observed at the end of the measurements [the difference in the interactions of GML and LA species is related, as already noticed, to the specifics of their molecular structures (cf. Figure S4)]. The synergistic competition for DOPC is especially well manifested at the equimolar GML/LA ratio. It is noteworthy that pearling instability is observed at this ratio and can be related with DOPC transport from buds to tubules. This transport reduces DOPC content, may result in a local increase of spontaneous curvature in bud patches, and can induce the formation of smaller buds with larger curvature.

In summary, we have demonstrated that mixtures of fatty acids and monoglycerides can exhibit synergistic membrane remodeling and the results offer physicochemical insight into the corresponding mechanism. In particular, our experiments revealed that a dynamic competition between membrane budding and tubule formation remodeling of the SLB platform occurs when there are similar concentrations of GML and LA within the GML/LA micelles, and this competition drives structural instability, including pearling behavior in some cases. At late stages, these processes are accompanied by membrane disruption. Taken together, our findings provide mechanistic insight into why fatty acids and monoglycerides can have synergistic biophysical and biological activities related to membrane disruption and support that mixtures of fatty acids and monoglycerides can be useful for application purposes. Notably, it has been estimated that the concentrations of GML[19] and LA[20,21] in human milk are around 11 and 10 mM, respectively, along with significant presence in other biological fluids and surfaces (e.g., skin[22]), so the importance of micellar aggregation on membrane remodeling processes observed in this study has potential biological relevance. From a broader perspective, the results presented also illustrate the richness of the phenomena that occur during coattachment of biological species. Other examples of this category include the formation of a protein corona around nanoparticles in biofluids[23] and competition for receptors during multivalent interaction of biological nanoparticles with phospholipid membranes.[24]

■ ASSOCIATED CONTENT

Supporting Information

The Supporting Information is available free of charge at https://pubs.acs.org/doi/10.1021/acs.jpclett.0c01138.

Experimental details; analysis of GML/LA mixing behavior; physicochemical model of bud and tubule formation; CMC measurement data; additional QCM-D data; chemical structures of DOPC, GML, and LA; and time-lapse fluorescence microscopy movies characterizing supported lipid bilayer interactions (PDF)

Supporting Movie S1: Real-time microscopic observation of 2000 μM LA addition to a supported lipid bilayer and resulting membrane morphological changes (AVI)

Supporting Movie S2: Real-time microscopic observation of 500 μM GML addition to a supported lipid bilayer and resulting membrane morphological changes (AVI)

Supporting Movie S3: Real-time microscopic observation of 500 μM GML and 31 μM LA coaddition to a supported lipid bilayer and resulting membrane morphological changes (AVI)

Supporting Movie S4: Real-time microscopic observation of 500 μM GML and 125 μM LA coaddition to a supported lipid bilayer and resulting membrane morphological changes (AVI)

Supporting Movie S5:Real-time microscopic observation of 500 μM GML and 500 μM LA coaddition to a supported lipid bilayer and resulting membrane morphological changes (AVI)

Supporting Movie S6: Real-time microscopic observation of 500 μM GML and 2000 μM LA coaddition to a supported lipid bilayer and resulting membrane morphological changes (AVI)

Supporting Movie S7: Real-time microscopic observation of irreversible pearling transition from a membrane bud (AVI)

Supporting Movie S8: Real-time microscopic observation of an irreversible membrane bud-to-tubule transition (AVI)

Supporting Movie S9: Real-time microscopic observation of an irreversible membrane tubule-to-bud transition (AVI)

Supporting Movie S10: Real-time microscopic observation of membrane disruption after buffer washing of a 2000 μM LA-treated supported lipid bilayer (AVI)

Supporting Movie S11: Real-time microscopic observation of membrane disruption after buffer washing of a 500 μM GML-treated supported lipid bilayer (AVI)

Supporting Movie S12: Real-time microscopic observation of membrane disruption after buffer washing of a 500/31 μM GML/LA-treated supported lipid bilayer (AVI)

Supporting Movie S13: Real-time microscopic observation of membrane disruption after buffer washing of a 500/125 μM GML/LA-treated supported lipid bilayer (AVI)

Supporting Movie S14: Real-time microscopic observation of membrane disruption after buffer washing of a 500/500 μM GML/LA-treated supported lipid bilayer (AVI)

Supporting Movie S15: Real-time microscopic observation of membrane disruption after buffer washing of a 500/2000 μM GML/LA-treated supported lipid bilayer (AVI)

■ AUTHOR INFORMATION

Corresponding Authors

Joshua A. Jackman − *School of Chemical Engineering, Sungkyunkwan University, Suwon 16419, Republic of Korea;*

https://dx.doi.org/10.1021/acs.jpclett.0c01138
J. Phys. Chem. Lett. 2020, 11, 4951−4957

orcid.org/0000-0002-1800-8102; Email: jjackman@skku.edu

Nam-Joon Cho − *School of Materials Science and Engineering, Nanyang Technological University, 637553, Singapore;* orcid.org/0000-0002-8692-8955; Email: njcho@ntu.edu.sg

Authors

Bo Kyeong Yoon − *School of Materials Science and Engineering, Nanyang Technological University, 637553, Singapore; School of Chemical Engineering, Sungkyunkwan University, Suwon 16419, Republic of Korea*

Soohyun Park − *School of Materials Science and Engineering, Nanyang Technological University, 637553, Singapore;* orcid.org/0000-0003-3261-7585

Gamaliel J. Ma − *School of Materials Science and Engineering, Nanyang Technological University, 637553, Singapore*

Kavoos Kolahdouzan − *School of Materials Science and Engineering, Nanyang Technological University, 637553, Singapore; Department of Chemistry, Pomona College, Claremont, California 91711, United States*

Vladimir P. Zhdanov − *Boreskov Institute of Catalysis, Russian Academy of Sciences, Novosibirsk 630090, Russia*

Complete contact information is available at: https://pubs.acs.org/10.1021/acs.jpclett.0c01138

Notes

The authors declare no competing financial interest.

■ ACKNOWLEDGMENTS

The authors thank Dr. Min Chul Kim for technical support with fluorescence microscopy experiments. This work was supported by the National Research Foundation of Singapore through a Proof-of-Concept grant (NRF2015NRF-POC0001-19), and by the National Research Foundation of Korea (NRF) grant funded by the Korean government (MSIT) (No. 2020R1C1C1004385). In addition, this work was supported by the Korea Research Fellowship Program through the National Research Foundation of Korea (NRF) funded by the Ministry of Science and ICT (2019H1D3A1A01070318).

■ ABBREVIATIONS

CMC, critical micelle concentration
DOPC, 1,2-dioleoyl-*sn*-glycero-3-phosphocholine
GML, glycerol monolaurate
LA, lauric acid
QCM-D, quartz crystal microbalance-dissipation
SLB, supported lipid bilayer

■ REFERENCES

(1) Thormar, H.; Hilmarsson, H. The Role of Microbicidal Lipids in Host Defense Against Pathogens and Their Potential as Therapeutic Agents. *Chem. Phys. Lipids* **2007**, *150*, 1−11.

(2) Royce, L. A.; Liu, P.; Stebbins, M. J.; Hanson, B. C.; Jarboe, L. R. The Damaging Effects of Short Chain Fatty Acids on *Escherichia coli* Membranes. *Appl. Microbiol. Biotechnol.* **2013**, *97*, 8317−8327.

(3) Maurer, S. E.; Deamer, D. W.; Boncella, J. M.; Monnard, P.-A. Chemical Evolution of Amphiphiles: Glycerol Monoacyl Derivatives Stabilize Plausible Prebiotic Membranes. *Astrobiology* **2009**, *9*, 979−987.

(4) Yoon, B. K.; Jackman, J. A.; Valle-González, E. R.; Cho, N.-J. Antibacterial Free Fatty Acids and Monoglycerides: Biological Activities, Experimental Testing, and Therapeutic Applications. *Int. J. Mol. Sci.* **2018**, *19*, 1114.

(5) Zhang, M. S.; Tran, P. M.; Wolff, A. J.; Tremblay, M. M.; Fosdick, M. G.; Houtman, J. C. D. Glycerol Monolaurate Induces Filopodia Formation by Disrupting the Association between LAT and SLP-76 Microclusters. *Sci. Signaling* **2018**, *11*, eaam9095.

(6) Thid, D.; Benkoski, J. J.; Svedhem, S.; Kasemo, B.; Gold, J. DHA-Induced Changes of Supported Lipid Membrane Morphology. *Langmuir* **2007**, *23*, 5878−5881.

(7) Hyldgaard, M.; Sutherland, D. S.; Sundh, M.; Mygind, T.; Meyer, R. L. Antimicrobial Mechanism of Monocaprylate. *Appl. Environ. Microbiol.* **2012**, *78*, 2957−2965.

(8) Yoon, B. K.; Jackman, J. A.; Kim, M. C.; Cho, N.-J. Spectrum of Membrane Morphological Responses to Antibacterial Fatty Acids and Related Surfactants. *Langmuir* **2015**, *31*, 10223−10232.

(9) Kawakami, L. M.; Yoon, B. K.; Jackman, J. A.; Knoll, W.; Weiss, P. S.; Cho, N.-J. Understanding How Sterols Regulate Membrane Remodeling in Supported Lipid Bilayers. *Langmuir* **2017**, *33*, 14756−14765.

(10) Batovska, D. I.; Todorova, I. T.; Tsvetkova, I. V.; Najdenski, H. M. Antibacterial Study of the Medium Chain Fatty Acids and Their 1-Monoglycerides: Individual Effects and Synergistic Relationships. *Polym. J. Microbiol.* **2009**, *58*, 43−47.

(11) Goddard, E. D.; Turro, N. J.; Kuo, P. L.; Ananthapadmanabhan, K. P. Fluorescence Probes for Critical Micelle Concentration Determination. *Langmuir* **1985**, *1*, 352−355.

(12) Shinoda, K.; Hutchinson, E. Pseudo-Phase Separation Model for Thermodynamic Calculations on Micellar Solutions. *J. Phys. Chem.* **1962**, *66*, 577−582.

(13) Granéli, A.; Edvardsson, M.; Höök, F. DNA-Based Formation of a Supported, Three-Dimensional Lipid Vesicle Matrix Probed by QCM-D and SPR. *ChemPhysChem* **2004**, *5*, 729−733.

(14) Lucklum, R.; Behling, C.; Hauptmann, P. Role of Mass Accumulation and Viscoelastic Film Properties for the Response of Acoustic-Wave-Based Chemical Sensors. *Anal. Chem.* **1999**, *71*, 2488−2496.

(15) Yu, Y.; Granick, S. Pearling of Lipid Vesicles Induced by Nanoparticles. *J. Am. Chem. Soc.* **2009**, *131*, 14158−14159.

(16) Jülicher, F.; Lipowsky, R. Domain-Induced Budding of Vesicles. *Phys. Rev. Lett.* **1993**, *70*, 2964−2967.

(17) Lipowsky, R. Domain-Induced Budding of Fluid Membranes. *Biophys. J.* **1993**, *64*, 1133−1138.

(18) Cebecauer, M.; Amaro, M.; Jurkiewicz, P.; Sarmento, M. J.; Šachl, R.; Cwiklik, L.; Hof, M. Membrane Lipid Nanodomains. *Chem. Rev.* **2018**, *118*, 11259−11297.

(19) Schlievert, P. M.; Kilgore, S. H.; Seo, K. S.; Leung, D. Y. M. Glycerol Monolaurate Contributes to the Antimicrobial and Anti-Inflammatory Activity of Human Milk. *Sci. Rep.* **2019**, *9*, 14550.

(20) German, J. B.; Dillard, C. J. Saturated Fats: A Perspective from Lactation and Milk Composition. *Lipids* **2010**, *45*, 915−923.

(21) Ballard, O.; Morrow, A. L. Human Milk Composition: Nutrients and Bioactive Factors. *Pediatr. Clin. North Am.* **2013**, *60*, 49−74.

(22) Fischer, C. L.; Blanchette, D. R.; Brogden, K. A.; Dawson, D. V.; Drake, D. R.; Hill, J. R.; Wertz, P. W. The Roles of Cutaneous Lipids in Host Defense. *Biochim. Biophys. Acta, Mol. Cell Biol. Lipids* **2014**, *1841*, 319−322.

(23) Docter, D.; Westmeier, D.; Markiewicz, M.; Stolte, S.; Knauer, S. K.; Stauber, R. H. The Nanoparticle Biomolecule Corona: Lessons Learned−Challenge Accepted? *Chem. Soc. Rev.* **2015**, *44*, 6094−6121.

(24) Parveen, N.; Rydell, G. E.; Larson, G.; Hytönen, V. P.; Zhdanov, V. P.; Höök, F.; Block, S. Competition for Membrane Receptors: Norovirus Detachment via Lectin Attachment. *J. Am. Chem. Soc.* **2019**, *141*, 16303−16311.